Supplementary Information
for

Seamless Cathode-Gel Electrolyte Interface Enables Highly Stable Aqueous Zinc Batteries

Yuguo Zheng,[a†] Liting Gao,[b†] Xin Liu, [a†] Yige Wang,[a] Jiahao li,[a] Jiachen Li,[b] Zhansheng Guo,[b*] Yizhou Zhang,[c*] Hanfeng Liang [a*]

[a]State Key Laboratory of Physical Chemistry of Solid Surfaces, College of Chemistry and Chemical Engineering, Xiamen University, Xiamen 361005, China
[b]Shanghai Institute of Applied Mathematics and Mechanics, School of Mechanics and Engineering Science, Shanghai Key Laboratory of Mechanics in Energy Engineering Shanghai University, Shanghai 200072, China
[c]Institute of Advanced Materials and Flexible Electronics (IAMFE), School of Chemistry and Materials Science, Nanjing University of Information Science & Technology, Nanjing 210044, China

[†]These authors contributed equally to this work.
*Corresponding author. Email: hfliang@xmu.edu.cn

Experimental section

Preparation of $Mg_{0.1}V_2O_5$ (MVO) nanobelts. The $Mg_{0.1}V_2O_5$·(MVO) nanobelts were synthesized using a simple hydrothermal method. In a typical procedure, 2 mmol of magnesium acetate, 4 mmol of ammonium metavanadate (AR), and 10 mL of acetic acid (AR) were added to 40 mL of deionized water and continuously stirred magnetically at 80°C until completely dissolved. The resulting solution was then transferred to a 100 mL Teflon-lined stainless-steel autoclave and maintained at 180°C for 48 h. Finally, the product was thoroughly washed with deionized water and dried at 60 °C for 12 h.

Preparation of MnO_2. For the synthesis of the MnO_2, 20 mmol of $KMnO_4$ and 30 mmol of $MnCl_2$ were separately dissolved in 200 mL de-ionized water. The $MnCl_2$ solution was gradually dropped into the $KMnO_4$ solution and stirred at room temperature for 10 h. The gradually brown precipitate was isolated via suction filtration, washed with water, dried at 80 °C for 8 hours, and subsequently annealed at 425 °C for 2 h in a muffle furnace.

Preparation of hydrogels. The 1%PAM-AA gel electrolyte was synthesized using a straightforward photopolymerization technique. Initially, 4 mg of Acrylic acid (AA, 98%) was dissolved in 2 mL of deionized water to form a 1 mol% AA solution. Subsequently, 0.75 g of Acrylamide (AM, 99.9%), 0.726 g of zinc trifluoromethanesulfonate (1 M $Zn(OTf)_2$), 2.5 mg of 2-hydroxy-4-(2-hydroxyethoxy)-2-methylpropiophenone (Irgacure 2959) and 1.5 mg of N,N'-methylene-bis(acrylamide) (MBAA) were added to the solution and sonicated until fully dissolved. Finally, the precursor solution was transferred into a designated mold, and the hydrogel electrolyte was obtained after 2 minutes of UV exposure.

In-situ photopolymerization achieves integrated cathode-gel electrolyte structure. To prepare the cathode slurry, 0.35 g of MVO, 0.1 g of Ketjen black, and 0.05 g of polyvinylidene fluoride (PVDF) were sequentially added to 2.5 mL of NMP and 0.4 mL of acrylic acid (AA) solvent. The slurry was uniformly coated onto a Ti foil and dried at 60 °C for 12 h to obtain the PA cathode. Additionally, 3 mg of N,N'-methylene-bis(acrylamide) (MBAA) and 5 mg of 2-hydroxy-4-(2-hydroxyethoxy)-2-methylpropiophenone (Irgacure 2959) were added to the cathode slurry. After coating onto a Ti foil (10 μm in thickness), the slurry was exposed to UV light for 2 minutes and dried at 60 °C for 12 h to obtain the Crosslinked cathode. The integration of the Pristine cathode with gel electrolyte (Integrated cathode) was achieved by coating a layer of precursor solution onto the Pristine cathode and irradiating it with UV light for 2 minutes.

Material characterization. Scanning electron microscope (SEM, Hitachi S-4800, Japan) was conducted to characterize the morphologies. The crystal structures were

probed via X-ray diffraction measurement (XRD, Rigaku IV, Japen) with a scan rate of 10° per minute. The concentration of dissolved manganese in the electrolyte was determined by an Inductively Coupled Plasma Optical Emission Spectrometer (ICP-MS, Agilent 7800, USA). Fourier-transform infrared spectroscopy (FTIR, Nicolet iS50, USA) was used to probe material molecular structures and chemical bonding. Utilizing nuclear magnetic resonance (NMR, Avance II 400M, Switzerland) to probe molecular structures.

Electrochemical measurements. The Zn||MnO_2 batteries and Zn||MVO batteries were assembled using coin cells (CR2032). The loading mass of active material is ~1.25 mg cm^2. The Zn foil with a thickness of 0.2 mm was polished with sandpaper and then cut into small pieces of 13 mm in diameter. The cyclic voltammetry (CV) curves were plotted on a CHI760E (CH Instruments, Shanghai) electrochemical workstation with a scan speed of 0.1 to 1.0 mV s^{-1} and the potential range from 0.2 to 1.6 V at room temperature. Ex-situ electrochemical impedance spectroscopy (EIS) was performed on a CHI760E (CH Instruments, Shanghai) electrochemical workstation. The frequency range was 0.01 Hz to 10 kHz and the amplitude was 5 mV. In-situ EIS was performed on a Bio-Logic VSP-3e (BioLogic, France) electrochemical workstation. The frequency range was 0.01 Hz to 20 kHz and the amplitude was 3 mV. The galvanostatic charge and discharge (GCD) test of the cells was carried out on a NEWARE Battery Test System (CT-4008Tn-5V20mA-164, Shenzhen, China) test system, with a potential range of 0.2 and 1.6 V and current densities from 0.1 to 1.0 A g^{-1}. The Galvanostatic Intermittent Titration Technique (GITT) was performed using a NEWARE Battery Test System (CT-4008Tn-5V20mA-164, Shenzhen, China) test system. The voltage window was 0.2 to 1.6 V, the constant current was 30 mA g^{-1}, and both the current pulse time and the relaxation time were 10 minutes.

Simulations. Our chemo-mechanical model based on the 2D porous electrode microstructure was established to describe the effects of in-situ and ex-situ electrolytes on the zinc ion diffusion, ion concentration distribution, and stress-strain behavior during discharge. The Zn^{2+} flux was used as an initial input, resulting in the increase of Zn^{2+} concentration of active particles and the subsequent influence on the mechanical modules including the stress-strain changes of active particles and electrolyte. All materials in the system are taken to be linearly elastic. The galvanostatic operation is using the following formula:

$$J = -i/(nF) \tag{S1}$$

In the equation, n is the unit normal vector of the surface of active material, F is Faraday's constant, and i is the surface current density. The gel electrolyte|interlayer| active material interface and active layer|current collector interface are assumed to be perfect bonded. For the conventional design, the initial zinc ion concentration is 0. The initial displacement field in the arbitrary region of electrode is 0.

Additional Figures and Data

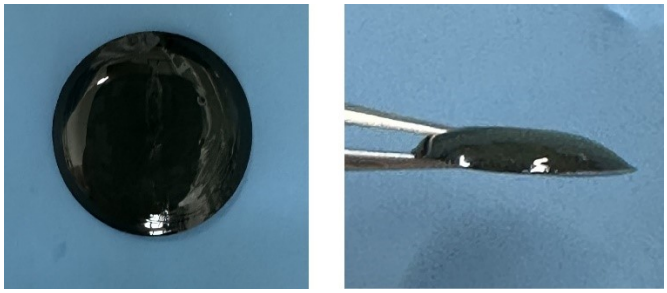

Fig. S1 Digital images of the integrated cathode.

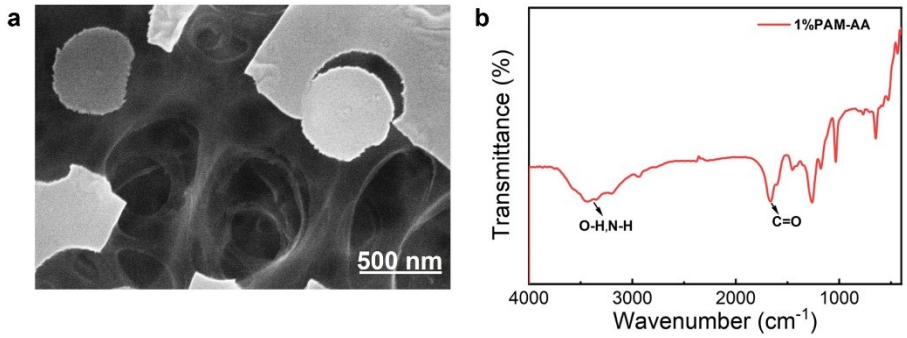

Fig. S2 (a) SEM image and (b) FT-IR spectrum of the as-prepared 1%PAM-AA hydrogel electrolyte.

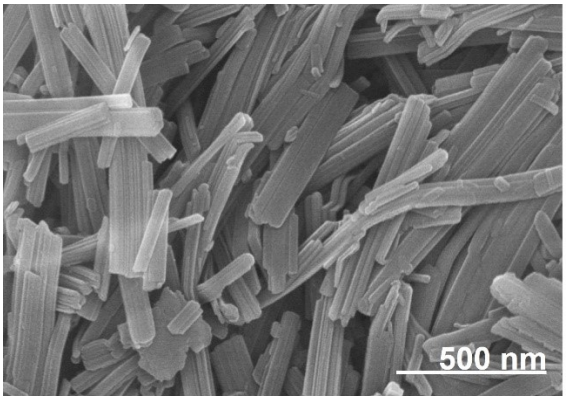

Fig. S3 SEM image of the as-prepared $Mg_{0.1}V_2O_5$ (MVO) particles.

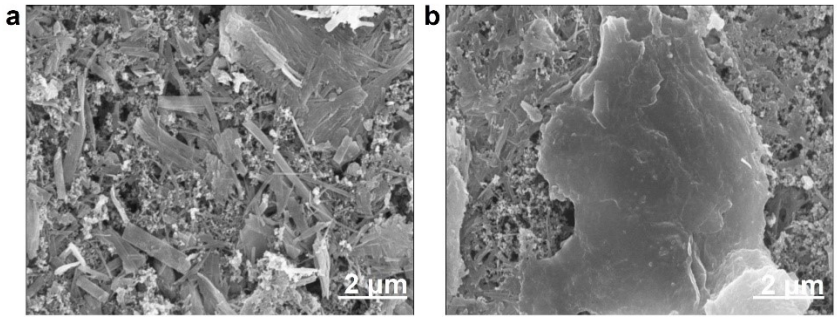

Fig. S4 SEM images of the (a) pristine and (b) crosslinked cathodes.

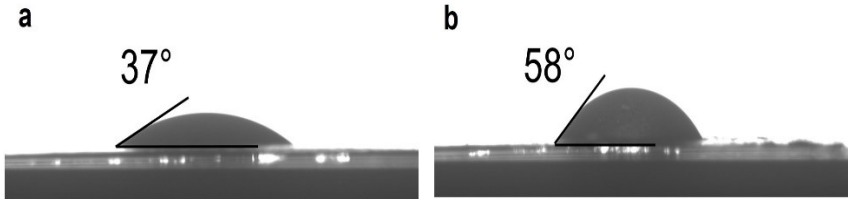

Fig. S5 Water contact angles of the (a) pristine and (b) crosslinked cathodes.

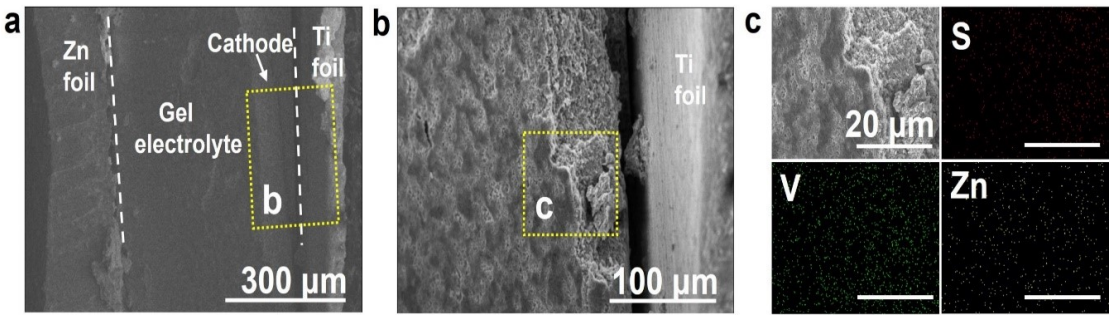

Fig. S6 (a,b) Cross-section SEM images of the integrated cathodes and the corresponding (c) EDS elemental maps.

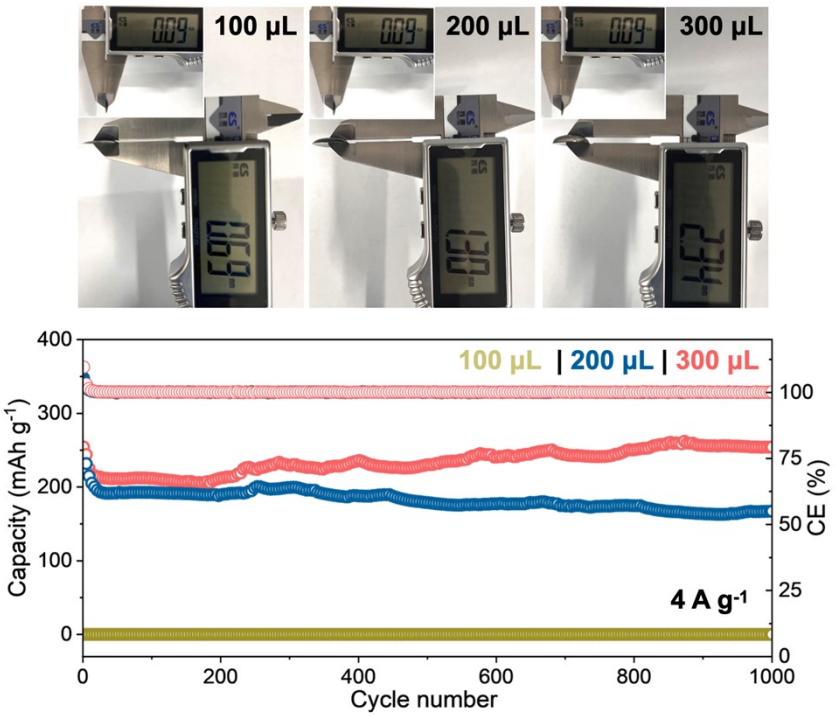

Fig. S7 Digital photos showing the thicknesses of Ti current collectors (insets) and integrated cathodes with different amounts of precursor solution (top panel). The cycling performance of integrated cathodes with different conditions at 4 A g^{-1} (bottom panel).

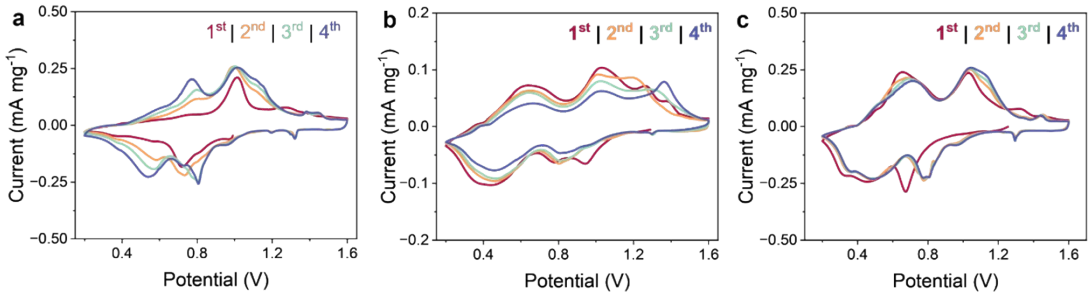

Fig. S8 CV profiles of the (a) pristine, (b) crosslinked, and (c) integrated cathodes at 0.1 mV s^{-1}.

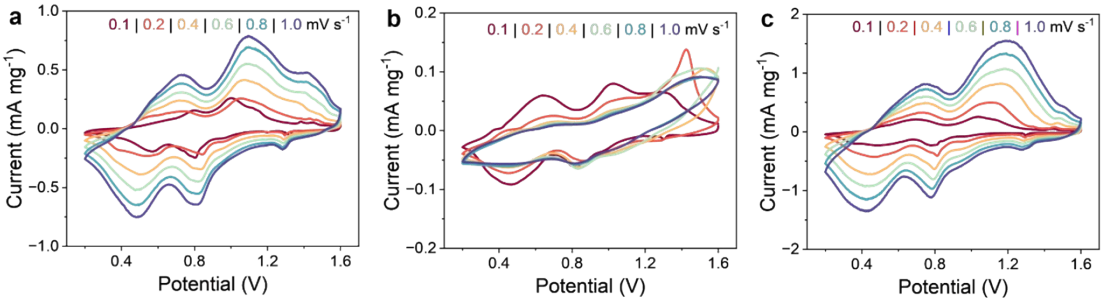

Fig. S9 CV profiles of (a) pristine, (b) crosslinked, and (c) integrated cathodes from 0.1-1.0 mV s^{-1}.

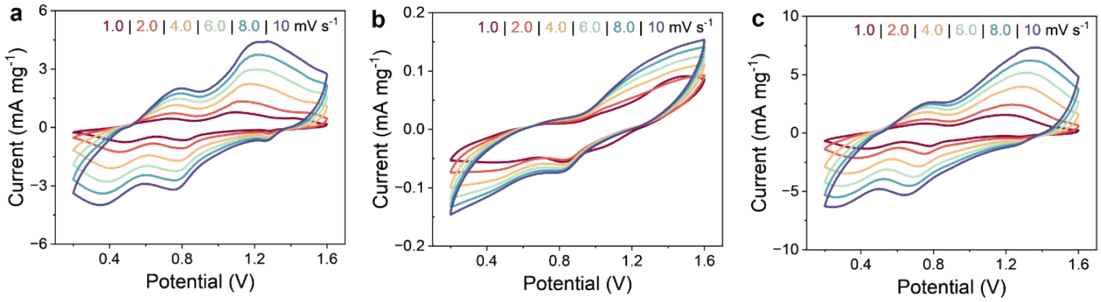

Fig. S10 CV profiles of (a) pristine, (b) crosslinked, and (c) integrated cathodes from 1.0-10 mV s^{-1}.

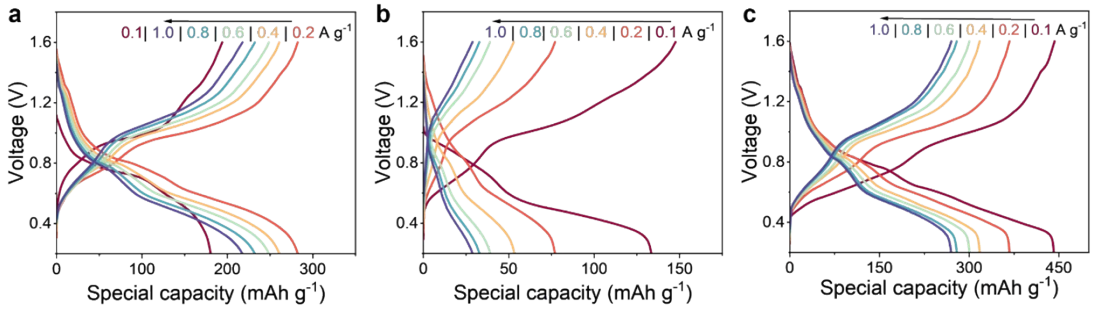

Fig. S11 GCD curves of (a) pristine, (b) crosslinked, and (c) integrated full batteries from 0.1-1.0 A g^{-1}.

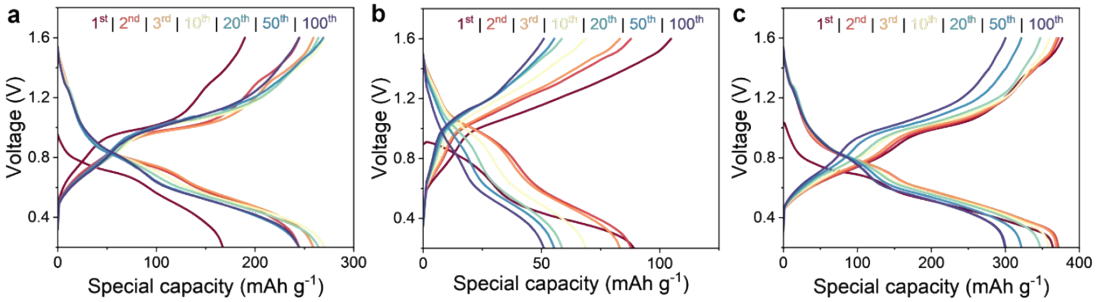

Fig. S12 GCD curves of (a) pristine, (b) crosslinked, and (c) integrated full batteries at 0.5 A g^{-1}.

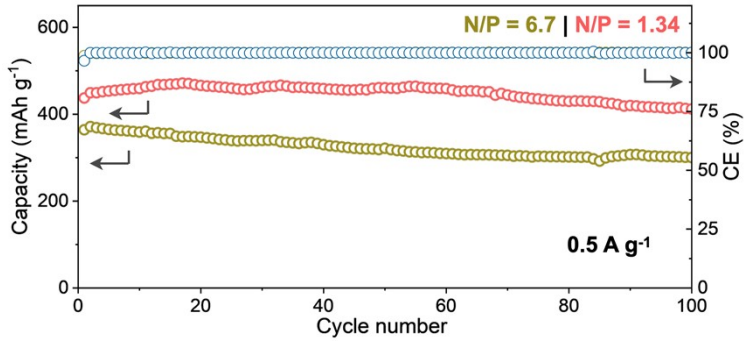

Fig. S13 Cycling performance of the integrated cathode at 0.5 A g^{-1} with different N/P ratios.

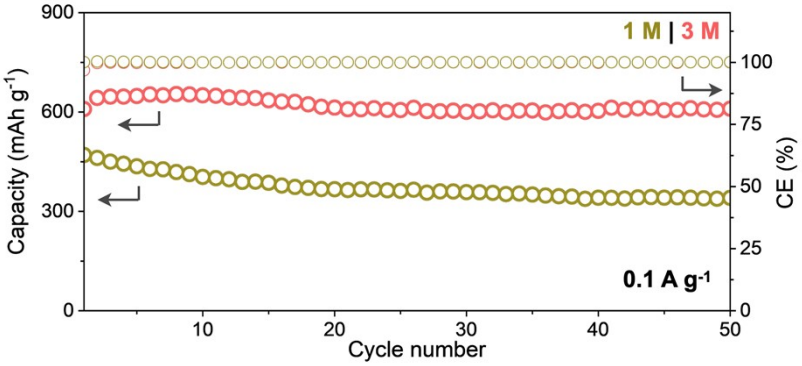

Fig. S14 Cycling performance of the integrated cathode in 1 M or 3 M $Zn(OTf)_2$ electrolytes at 0.1 A g^{-1}.

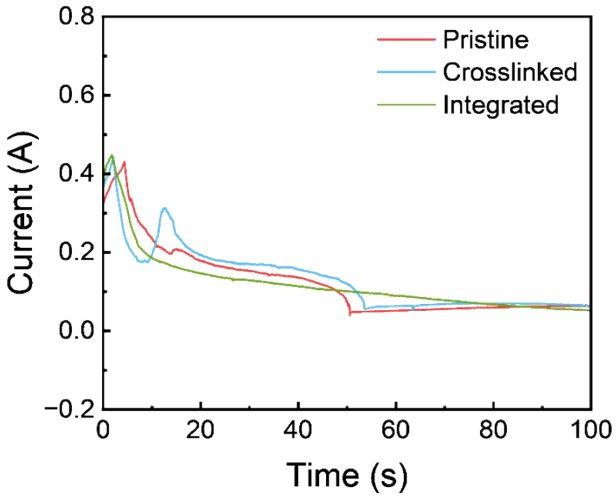

Fig. S15 The current against time curves for the three positive electrodes under a constant voltage.

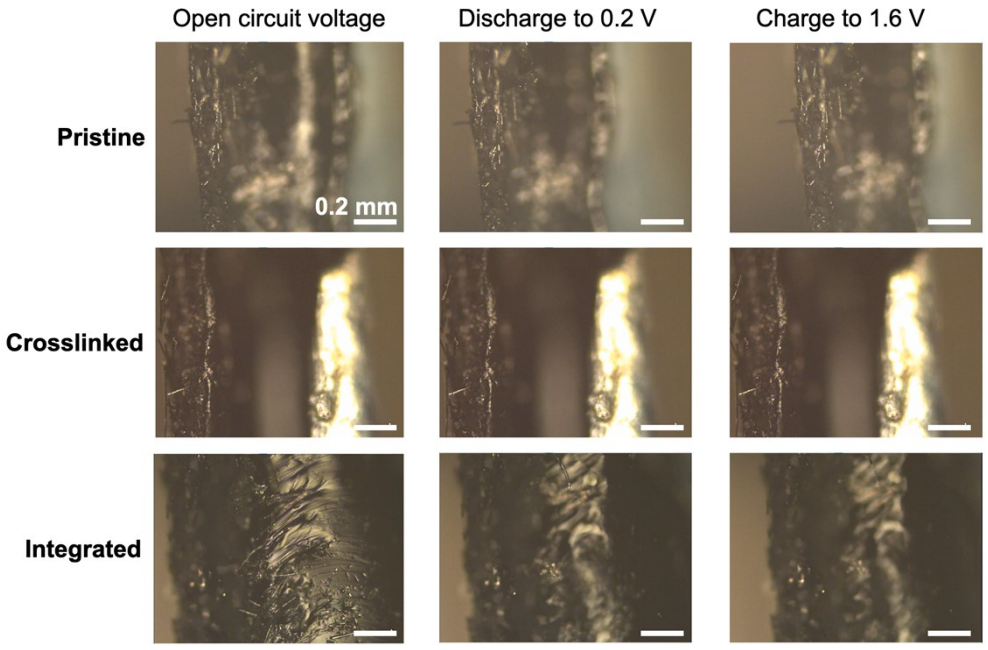

Fig. S16 *In-situ* optical microscopy observation of the cathode-gel interfaces in different cathodes during cycling.

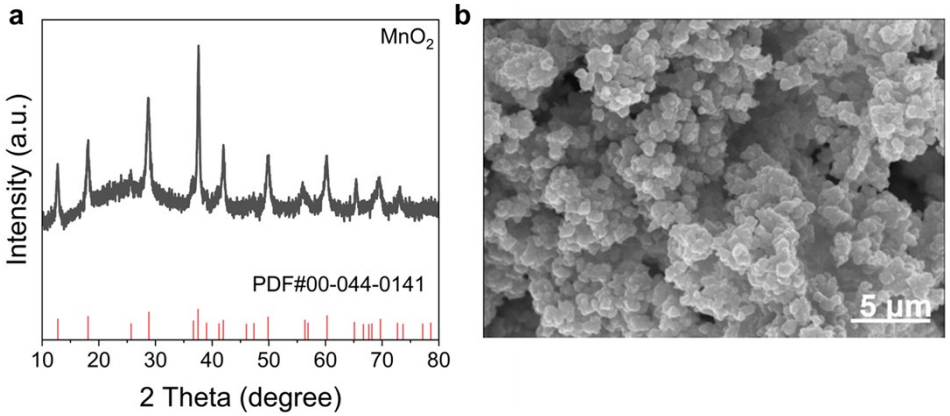

Fig. S17 (a) XRD pattern and (b) SEM image of the as-prepared MnO_2 particles.

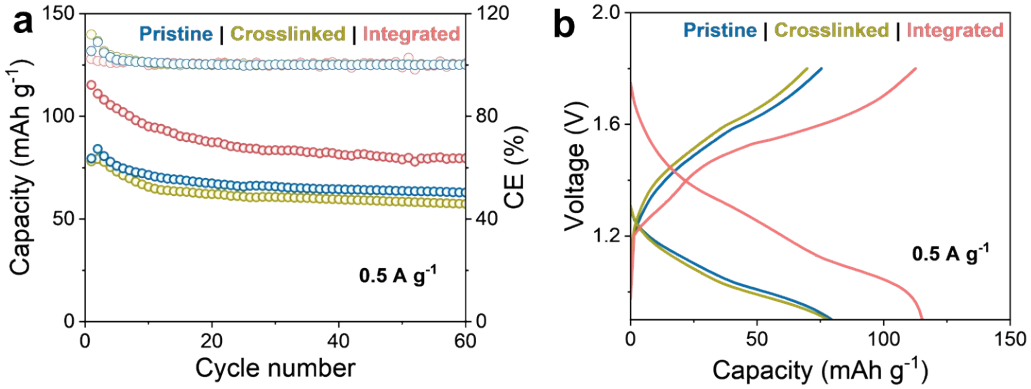

Fig. S18 (a) Cycling performance and (b) The first cycle GCD curves of Zn||MnO_2 full batteries with 1 M $Zn(OTf)_2$.

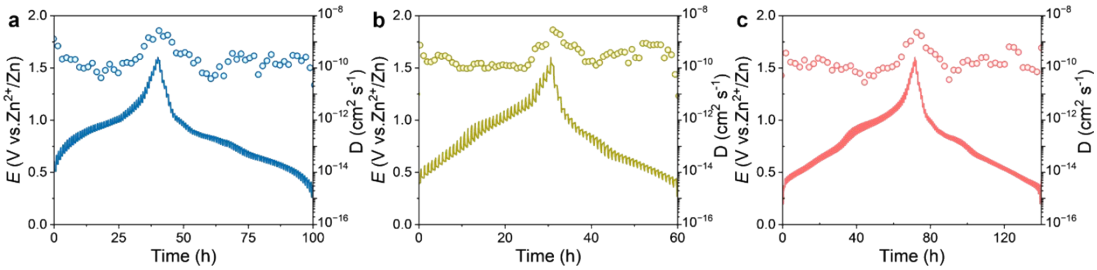

Fig. S19 GITT profiles of (a) pristine, (b) crosslinked, and (c) integrated cathodes.

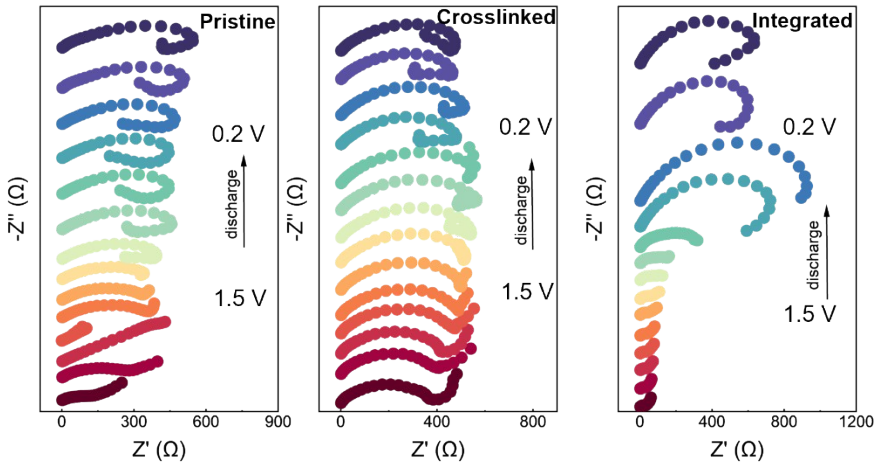

Fig. S20 *In-situ* EIS spectra of (a) pristine, (b) crosslinked, and (c) integrated cathodes.

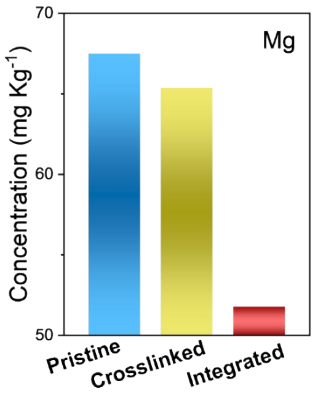

Fig. S21 Quantification of dissolved Magnesium in hydrogel electrolyte